Adv Syst Sci Appl 2025; **3**; 11-24
Published online at https://ijassa.ipu.ru.

Study of the Effects of Axially Defective Blades of Wind Turbine on Vibration Patterns

Abdulhamid Hamdan Al-Hinai*, Karu Clement Varaprasad, Vinod Kumar

Sohar University, Sohar, Sultanate of Oman

Abstract: Axial defects in wind turbine blades represent a critical factor influencing both their vibration characteristics and overall operational performance. Among these, the axial cracks are particularly concerning. They alter the structural dynamics of the blade, compromise stiffness and reduce the ability of the system to withstand fluctuating aerodynamic and mechanical loads. This study presents a systematic vibration analysis of wind turbine blades with three different levels of axial crack defects, specifically of lengths 50 mm, 100 mm, and 350 mm subjected to shaft rotational speeds ranging from 50 rpm to 200 rpm. The experimental investigations are conducted using the Spectra Quest wind turbine simulator. It replicates the conditions of a real wind turbine by incorporating actual wind data from Sohar. The results reveal a strong correlation between defect size, shaft speed and vibration response with regression analysis yielding a high coefficient of determination ($R^2 = 0.98$). Further, Taguchi design of experiments is applied to identify the most effective parameter combinations for minimizing vibration risks. The proposed condition monitoring framework demonstrates an effective approach for detecting and mitigating vibration levels in defective blades. Thereby contributing to enhanced reliability, extended service life and reduced maintenance costs in wind turbine systems.

Keywords: Blade Defect, Crack size, Rotational Speed, Taguchi analysis, Vibration Patterns, Wind Turbine.

1. INTRODUCTION

The quick development of wind energy as a clean and renewable control source has led to expanded attention to upgrading the reliability and efficiency of wind turbine systems [1]. Regardless of significant advancements in wind turbine innovation, the presence of blade defects remains a challenge, affecting the execution and life expectancy of wind turbines [2]. Blade vibration can be categorized into three types: stall flutter, classical flutter, and axial vibration. These vibrations can cause severe damage to the blade structure.

The wind turbine blades are essential components that convert the kinetic energy of the wind into a mechanical form of energy. As these blades are subjected to significant mechanical loads and environmental forces throughout their working lives, they are critical to the longevity and productivity of wind energy systems. [3]. However, the presence of defects inside these blades, especially along the axial direction, can compromise structural integrity and performance, leading to operational downtime, upkeep costs, and security risks [4][5]. Axial defects, such as axial cracks, can lead to catastrophic failures if not detected and treated on time. Vibration-based investigation of wind turbines utilizes advanced monitoring methods to assess blade integrity and performance. Data complexity and computational requirements are some challenges in vibration-based analysis. Vibration analysis procedures, such as time domain and regression analysis, are employed to detect and analyze these defects, allowing for timely maintenance and repair interventions to prevent costly downtime and ensure the safe operation of wind turbines [6]. This is particularly useful for detecting sudden changes in vibration patterns and blade failures. Regression analysis of vibration data involves modelling the relationship between various vibration parameters and the condition of wind turbine blades.

* Corresponding author: abdulhamidalhinai@gmail.com

Taguchi analysis is a statistical method used in this paper for optimizing the wind turbine performance as it is widely used in engineering research [7]. The main idea of this method is to design experiments efficiently so that it shows how different input factors affect the output [8]. This is done while minimizing variation (noise) and maximizing performance [9]. This analytical approach aims to correlate vibration measurements with the health status of the blades under different operating conditions. This can identify patterns and trends in vibration data indicative of potential defects or deterioration. These vibration amplitudes and frequencies may signal abnormalities or wear in turbine blades. Condition monitoring procedures allow for proactive evaluation of turbine component health, enabling early defect detection and targeted maintenance interventions [10]. Wind turbines are becoming increasingly larger in capacity [11]. This proactive maintenance technique empowers convenient intervention, reducing downtime, maintenance costs, and safety risks while optimizing energy generation and increasing the operational life expectancy of wind turbines. This research paper presents an analytical vibration analysis of axially defective wind turbine blades through time domain and regression analyses, as a condition monitoring approach. The novelty of this research study is to simulate Sohar's actual wind speed data using a vibration lab wind turbine simulator to evaluate the vibration patterns of a wind turbine due to axially defective blades.

2. LITERATURE REVIEW

Currently, many research studies on blade vibration suppression focus on passive and active control methods. Passive control adjusts the mass and stiffness distribution of the blade structure, changes the blade's natural frequency, redesigns the blade structure, and replaces blade materials. Lighter and harder carbon fibers were used to improve blade performance. The results showed that the new materials can reduce vibration speed by about 5% to ensure a certain bend-twist coupling [12]. Active control suppresses blade vibration by installing dampers on the original blade and using advanced control strategies without adjusting the structure, designing new airfoils, or replacing blade materials. A new tuned damper was proposed to be installed inside the blade to improve the critical condition of blade vibration. The results showed that the tuned damper can increase the critical speed of blade flutter by 100% [13]. However, this method was mainly for the blade torsional flutter problem, rather than the axial vibration. An active optimal control scheme based on a piezoelectric actuator and linear rectangular Gaussian theory was proposed to suppress wave vibration [14]. Researchers aimed to decrease the vibration amplitude by reducing the fluctuations of the axial force moment [15][16][17]. Additionally, as the blade vibrates, it is necessary to detect the vibration and modify the load control algorithm by identifying the blade dynamics [18].

Blade vibration, which generally involves axial vibration, is related to the inherent dynamic characteristics and blade aerodynamic characteristics. However, there are still some deficiencies in current research on blade vibration due to various defect directions. With the increase in blade length, wind shear and tower shadow effects on blade vibration will become more prominent. Therefore, it is worth considering how to prevent blade vibration caused by different effects. This paper investigates the analysis of blade vibration caused by axial defects and the effective optimization methods to suppress blade vibration.

3. METHODOLOGY

The research work involves wind speed data collection followed by practical design and setup for test measurement and signal processing. Design of tests and model development are then employed. Results are discussed through time-domain and analytical vibration analysis, alongside graphical analysis. Regression and Taguchi analyses are conducted to further understand vibration patterns. Finally, prediction, optimization, and sensitivity analyses are

performed to enhance comprehension of the effects of axially defective blades on wind turbine vibration. Fig. 3.1 shows the methodology flow chart.

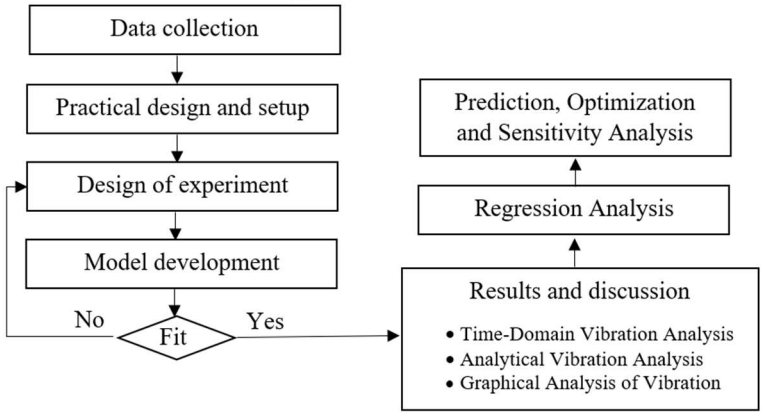

Fig. 3.1. Methodology flow chart

3.1. Data Collection

The Spectra Quest wind turbine simulator is a lab facility installed in the vibration lab at Sohar University, Oman. The Sohar town's monthly average wind speed is shown in Table 3.1, which was measured at a height of 50 m using Sohar University facilities. Using the wind speed to rotational speed conversion for the Spectra Quest wind turbine simulator, the wind speed data was converted to a rotational speed at the low-speed shaft. Then, this rotational speed was converted to a high-speed shaft rotational speed, at which the accelerometer was mounted, using the gearbox ratio of 4.571. A conversion error of 5% is considered in the Spectra Quest wind turbine simulator.

The high-speed shaft rotational speed in Table 3.1 ranges from almost 100 rpm to 150 rpm. To represent it clearly, a hypothetical range of rotational speed from 50 rpm to 200 rpm is proposed, considering the 50 rpm limit on both sides. Considering an interval speed range of 50 rpm, the set of input rotational speeds is namely; 50 rpm, 100 rpm, 150 rpm and 200 rpm for the current research work. This research work includes practical design and setup, data measurement and signal processing methods, and vibration analysis techniques. The practical work was done by installing the axially defective wind turbine blades, one after the other, in the Spectra Quest wind turbine simulator and obtaining the resultant vibration patterns under the input set of rotational speeds. Graphical representation and regression analysis were employed to correlate with the condition monitoring approach.

Table 3.1. Monthly averaged wind speed and corresponding rotational speeds

Months	Average wind speed (m/s)	Low shaft speed (rpm)	High shaft speed (rpm)
Jan	4.50	24.75	113.15
Feb	5.12	28.16	128.74
Mar	4.87	26.79	122.45
Apr	4.80	26.40	120.69
May	5.47	30.09	137.54
Jun	5.47	30.09	137.54
Jul	5.35	29.43	134.52
Aug	5.15	28.33	129.49
Sep	4.92	27.06	123.71
Oct	4.24	23.32	106.61
Nov	3.86	21.23	97.06
Dec	4.42	24.31	111.14

3.2. Practical Design and Setup

The Spectra Quest wind turbine simulator is a wind turbine lab facility with three blades. One of these blades was replaced by an axially defective blade for each test. Based on the crack size, there are three different blades with different crack sizes, namely; low, medium and high. These axial defects were intentionally made for analysis purposes. After replacing the healthy blade with a defective blade, the system was tested for vibration analysis. The same was repeated using medium and high defective blades at each time. This simulator provides a lab-wise controlled environment for replicating real-world conditions, enabling precise testing and data collection.

The varying rotational speeds were measured using a tachometer installed in the Spectra Quest wind turbine simulator, while the vibration level was measured by an accelerometer installed at the high-speed shaft of the Spectra Quest wind turbine simulator. Each accelerometer measures the vibrational excitation in one direction [10].

The sensor's readings are collected by a data acquisition system that is connected to a computer. Vibra Quest signal analysis software is used to analyze the signals the data acquisition system reads and generate output vibration reports.

3.3. Design of Experiments

Design of experiments (DoE) is a systematic approach utilized to optimize processes and products by exploring the effects of various factors and their interactions. Table 3.2 outlines the input parameters and their corresponding levels needed for conducting an effective design of experiments. These parameters include defect level with low, medium, and high categories, defect size with values of $50\text{mm} \leq x_1 \leq 350\text{mm}$, and shaft rotational speed with options of $50\text{rpm} \leq x_2 \leq 200\text{rpm}$. The impact of these inputs on vibration patterns can be evaluated by manipulating them at different levels. This facilitates the identification of optimal settings to enhance efficiency and reduce vibration levels.

Table 3.2. Input parameters and their levels

Parameters	Input	Levels			
Defect Level		Low	Medium		High
Defect size (mm)	x1	50	100		350
Shaft rotational speed (rpm)	x2	50	100	150	200

3.4. Model Development

To optimize machine learning model development for wind turbine performance, a multifaceted approach integrating wind to rotational speed conversion and crack size vibration effects is essential. Leveraging monthly averaged wind speeds and corresponding rotational speeds in Table 3.1 provides a foundational dataset for training and validation. Additionally, the input parameters and their levels in Table 3.2 offer critical variables for model refinement. These data can be analyzed to predict optimal shaft speeds based on wind conditions and detect potential defects by harnessing advanced algorithms, including regression analysis. This holistic optimization strategy not only enhances turbine efficiency but also minimizes maintenance costs and downtime, contributing to sustainable energy production.

4. RESULTS AND DISCUSSION

The Vibra Quest software exported the vibration results in MS Excel format, after reading the data from the vibration sensor (accelerometer). At the same time, the software shows the time-domain vibration waveforms with the times of a maximum of two time-peaks set by the software. For each test, the generated file presents about 32768 vibration peaks (positive and negative waveform peaks) that were used for vibration analysis. In this results section, the time domain waveforms are discussed for each case of the defective blades (low, medium and high)

run at each rotational speed (50 rpm, 100 rpm, 150 rpm and 200 rpm) followed by the analytical analysis of the vibration patterns. After that, the graphical and regression analyses are discussed. Finally, the vibration model optimization is discussed for prediction and sensitivity analysis.

4.1. Time-Domain Vibration Analysis

The practical tests of the vibration analysis presented the vibration patterns obtained by the accelerometer at different rotational speeds using the Vibra Quest wind turbine simulation system. At each case of defect size, four tests were performed at each rotational speed (50 rpm, 100 rpm, 150 rpm and 200 rpm) respectively.

4.1.1. Case 1: Low Defective Blade

The Spectra Quest wind turbine simulation system operated first with two healthy blades and one low defective blade. Figs. 4.1 to 4.4 show the vibration waveform readings at each rotational speed respectively, generated by Vibra Quest software. As the rotational speed increases, the amplitude of the vibration level increases. The Figs. show also the pre-set two-time times when higher values of amplitudes occur.

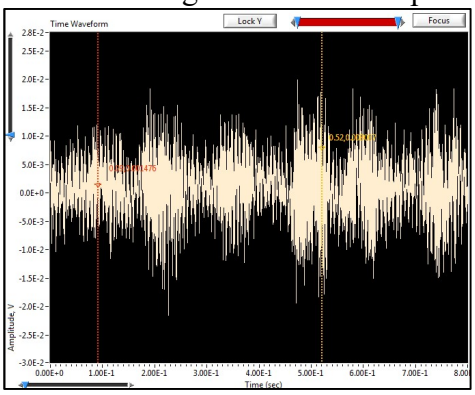

Fig. 4.1. Vibration waveform with a low defective blade at 50 rpm

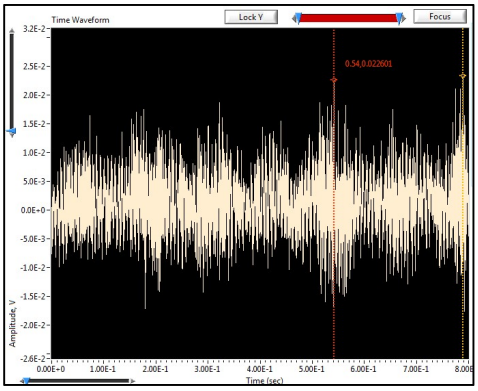

Fig. 4.2. Vibration waveform with a low defective blade at 100 rpm

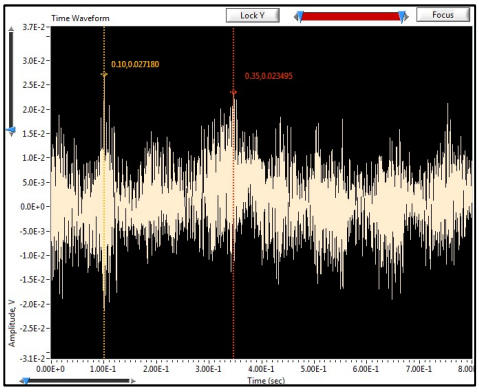

Fig. 4.3. Vibration waveform with a low defective blade at 150 rpm

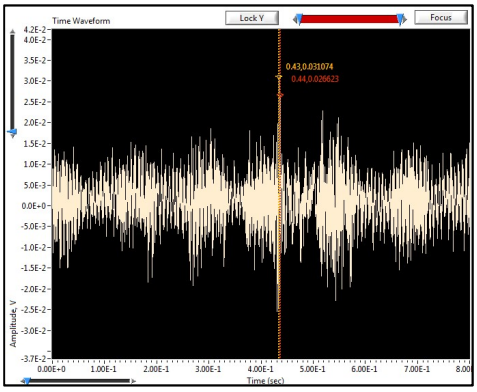

Fig. 4.4. Vibration waveform with a low defective blade at 200 rpm

4.1.2. Case 2: Medium Defective Blade

In this case, the low defective blade is replaced by a medium defective blade. The Spectra Quest wind turbine simulation system is operated with two healthy blades and one medium defective blade. Figs. 4.5 to 4.8 show the vibration waveform readings at each rotational speed respectively. Same as in case 1, the amplitude of the vibration level increases with the increase in rotational speed. The times when higher values of amplitudes occur are shown also in these Figs.

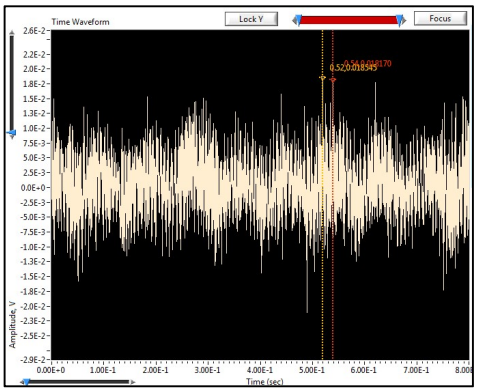

Fig. 4.5. Vibration waveform with a medium defective blade at 50 rpm

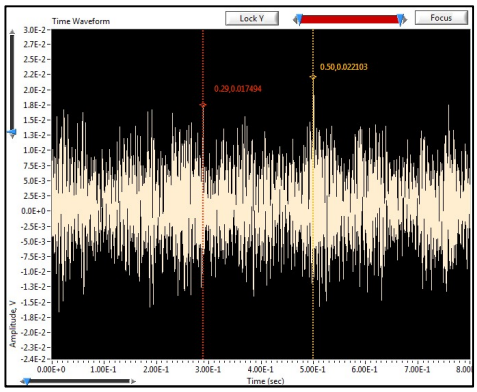

Fig. 4.6. Vibration waveform with a medium defective blade at 100 rpm

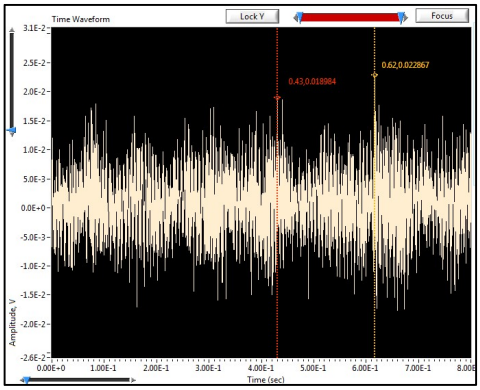

Fig. 4.7. Vibration waveform with a medium defective blade at 150 rpm

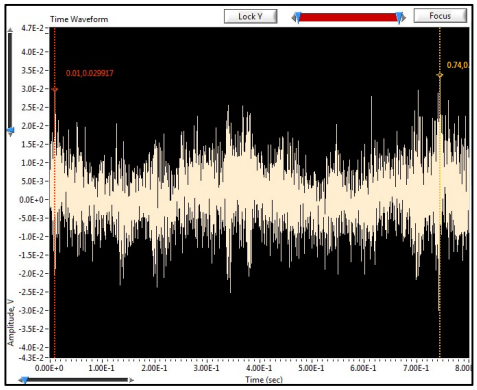

Fig. 4.8. Vibration waveform with a medium defective blade at 200 rpm

4.1.3. Case 3: High Defective Blade

In case 3, the Spectra Quest wind turbine simulation system operated with two healthy blades and one high defective blade. Figs. 4.9 to 4.12 show the vibration waveform readings at each rotational speed respectively. The same as in cases 1 and 2, the amplitude of the vibration level increases as the rotational speed increases. These graphs also display the times at which the amplitudes reach larger values.

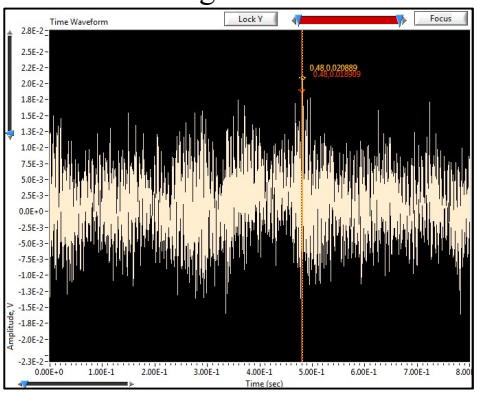

Fig. 4.9. Vibration waveform with a high defective blade at 50 rpm

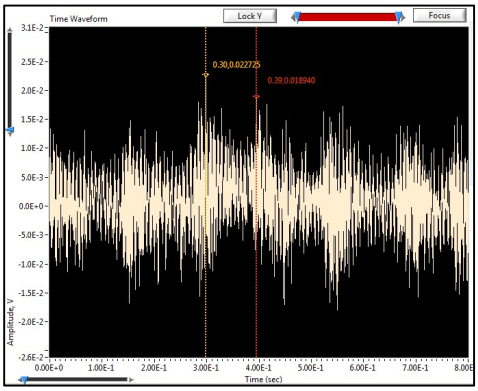

Fig. 4.10. Vibration waveform with a high defective blade at 100 rpm

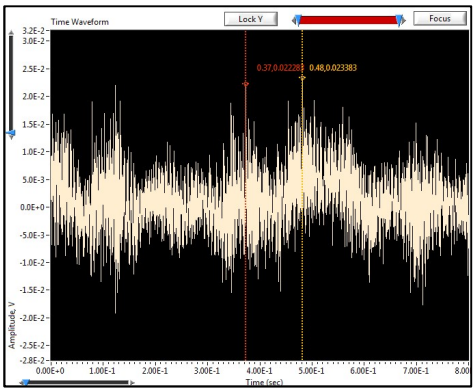

Fig. 4.11. Vibration waveform with a high defective blade at 150 rpm

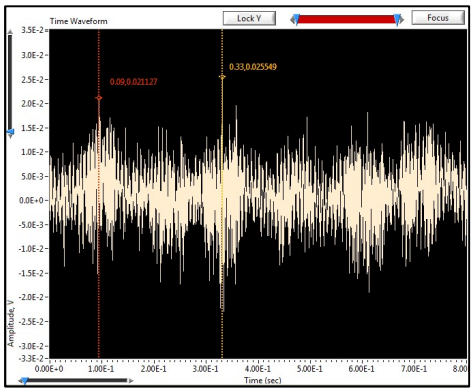

Fig. 4.12. Vibration waveform with a high defective blade at 200 rpm

4.2. Analytical Vibration Analysis

For this research work, the Vibra Quest software generated the vibration patterns in the voltage unit. For each test, about 32768 vibration peaks (positive and negative) were generated by the software. An analytical analysis was conducted including the minimum (Min) and maximum (Max) peak values, the averages of (n) negative peaks (Avg. (Min)) and (m) positive peaks (Avg. (Max)). Additionally, determining the vibration range, spanning from the average of positive peaks to the average of negative peaks shows the amplitude dispersion within the recorded data. Table 4.1 tabulates these results from the generated reports. For each test, the following equations were used:

$$Avg.(Min) = \frac{\sum_{i=1}^{n}(negative\ vibration\ peaks)}{n} \tag{4.1}$$

$$Avg.(Max) = \frac{\sum_{i=1}^{m}(positve\ vibration\ peaks)}{m} \tag{4.2}$$

$$Vibration\ Range\ = Avg.(Max) - Avg.(Min) \tag{4.3}$$

Table 4.1. Vibration waveform results

Test	Input Parameters			Vibration waveform analysis				
	Defect Level	Defect size (mm)	Rot. Speed (rpm)	Min (V)	Max (V)	Avg. (Min) (V)	Avg. (Max) (V)	Vibration Range (V)
1	Low	50	50	-0.028766	0.025389	-0.004481	0.004612	0.009093
2	Low	50	100	-0.080538	0.075132	-0.015803	0.015027	0.030830
3	Low	50	150	-0.150698	0.122752	-0.017426	0.017276	0.034702
4	Low	50	200	-0.141121	0.169997	-0.019577	0.019999	0.039577
5	Medium	100	50	-0.025456	0.024302	-0.004495	0.004679	0.009174
6	Medium	100	100	-0.077624	0.069251	-0.015792	0.015070	0.030862
7	Medium	100	150	-0.207226	0.144662	-0.019152	0.018824	0.037976
8	Medium	100	200	-0.144500	0.148000	-0.021969	0.022760	0.044729
9	High	350	50	-0.023882	0.027492	-0.004298	0.004885	0.009183
10	High	350	100	-0.076275	0.065869	-0.016437	0.014879	0.031316
11	High	350	150	-0.148958	0.135611	-0.020603	0.020607	0.041210
12	High	350	200	-0.200616	0.177882	-0.022574	0.023095	0.045668

As shown in Table 4.1, the tests investigate how the vibration waveform features are affected by different rotation speeds and defect sizes. The generated waveforms are examined in terms of their minimum peaks, maximum peaks, average of minimum peaks, average of maximum peaks, and the range from maximum to minimum average peaks for every combination of parameters. The range of average peaks widens as the rotation speed increases at each defect level.

At a low defect level, as the rotation speed increases from 50 to 200 rpm, there is a gradual expansion in the range of average vibration. For instance, as shown in Fig. 4.1, where the defect size is 50 mm, the range of average voltages increases from 0.009093 V at 50 rpm to 0.039577 V at 200 rpm, as shown in Fig. 4.4. This expansion suggests that higher rotation speeds exacerbate vibration fluctuations, likely due to increased stress and deformation within the system. Similarly, at medium and high defect levels, the range of average voltages exhibits a notable increase as both defect size and rotation speed rise, as shown in Figs. 4.5 to 4.8 for a medium defective blade and Figs. 4.9 to 4.12 for a high defective blade.

4.3. Graphical Analysis of Vibration

The collected vibration data is graphically analyzed in Fig. 4.13 to represent the peak-peak levels. The graphs show the relationship between vibration levels in terms of defect size and rotational speed. As the rotational speed increases, the vibration level increases for each defect size. The higher the defect size, the higher the vibration level at the same rotational speed.

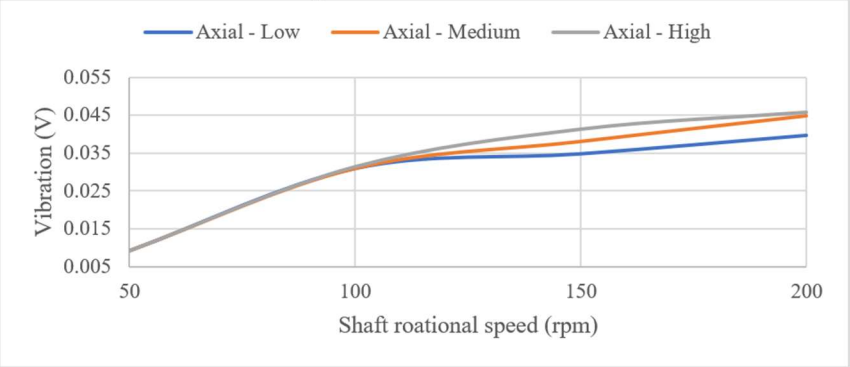

Fig. 4.13. Peak-peak vibration

The presented graphs in Fig. 4.13 reflect the dynamic behavior of the wind turbine system. Till 100 rpm rotational speed, the graphs are almost linearly parallel and then they vary due to either non-linear response of the system, resonance effects, non-linearities in the defects or dynamic response of the system. Table 4.2 presents a comparison of vibration levels for each defect level with the average vibration level across each rotational speed. The higher the crack size, the higher the vibration level. However, as rotational speed increases, the impact of crack severity becomes more pronounced, with higher speeds exacerbating vibration levels, particularly evident in cases of medium and high crack severities.

Table 4.2. Vibration levels comparison

Rotational speed (rpm)	Average vibration (V)	Low crack vibration (V)	Medium crack vibration (V)	High crack vibration (V)
50	0.009150	0.009093	0.009174	0.009183
100	0.031002	0.030830	0.030862	0.031316
150	0.037963	0.034702	0.037976	0.041210
200	0.043325	0.039577	0.044729	0.045668

4.4. Regression Analysis of Vibration

Regression analysis is performed to quantify the relationship between defect size and shaft rotational speeds with vibration levels. The quadratic function represents the best regression expression for the research model compared with linear regression. Table 4.3 shows the input factors and output response set for the quadratic regression model.

Table 4.3. Input and output parameters for a quadratic regression model

Crack Size (mm)	Crack Size^2 (mm^2)	Rot. Speed (rpm)	Rot. Speed^2 (rpm^2)	Crack Size × Rot. Speed (mm × rpm)	Vibration range (V)
50	2500	50	2500	2500	0.009093
50	2500	100	10000	5000	0.030830

50	2500	150	22500	7500	0.034702
50	2500	200	40000	10000	0.039577
100	10000	50	2500	5000	0.009174
100	10000	100	10000	10000	0.030862
100	10000	150	22500	15000	0.037976
100	10000	200	40000	20000	0.044729
350	122500	50	2500	17500	0.009183
350	122500	100	10000	35000	0.031316
350	122500	150	22500	52500	0.041210
350	122500	200	40000	70000	0.045668

The quadratic regression analysis was performed using Minitab software. Table 4.4 gives the regression statistics of the regression model.

Table 4.4. Regression Statistics

Multiple R	R Square	Adjusted R Square	Standard Error	Observations
0.990879	0. 981841	0. 966708	0. 002504	12

As shown in Table 4.4, the Multiple R of 0.990879 indicates a strong positive and direct relationship between the independent variables (defect size and rotational speeds) and the dependent variable (vibration level). The R Square of 0.981841 shows that approximately 98.18% of the variance in the vibration level is clarified by the defect size and rotational speeds in the regression model. The Adjusted R Square is calculated as 0.966708, slightly lower than the R Square, showing that the model may have some degree of overfitting. The Standard Error of 0.25% indicates the average amount of error in the predicted values of the vibration level.

The analysis of variance (ANOVA) in this research work is conducted to evaluate the implications of the regression model and its components. This statistical technique helps determine if the observed variations in vibration levels can be attributed to the different defect sizes tested. Table 4.5 shows the ANOVA results and Table 4.6 shows the regression summary.

The ANOVA table offers a clear understanding of the effects of vibration caused by axially defective blades at different rotation speeds, ranging from 50 to 200 rpm. The F-statistic of 64.88 indicates a strong correlation between rotation speed and vibration caused by defective blades. Additionally, the Significance F value of 3.85×10^{-5} suggests that this correlation is statistically significant, reinforcing the idea that changes in rotation speed affect vibration caused by axially defective blades.

Table 4.5. Analysis of Variance (ANOVA)

	df	SS	MS	F	Significance F
Regression	5	0.002034	0.000407	64.88184	3.85×10^{-5}
Residual	6	3.76×10^{-5}	6.27×10^{-6}		
Total	11	0.002071			

Table 4.6. Regression Summary

	Coefficients	Standard Error	t Stat	P-value
Intercept	-0.02011	0.005763	-3.48954	0.012991
Crack Size	5.73×10^{-5}	6.5×10^{-5}	0.881162	0.412133
Crack Size^2	-1.6×10^{-7}	1.58×10^{-7}	-1.0019	0.355069
Rot. Speed	0.000612	7.51×10^{-5}	8.139658	0.000185
Rot. Speed^2	-1.6×10^{-6}	2.89×10^{-7}	-5.70372	0.001256
Crack Size × Rot. Speed	1.23×10^{-7}	1×10^{-7}	1.224465	0.266668

The regression equation derived from this analysis offers a mathematical model for predicting vibration levels (peak-peak) based on defect size and shaft rotational speed:

$$\text{Vibration level} = -0.02011 + 5.73 \times 10^{-5} x_1 - 1.6 \times 10^{-7} x_1^2 + 0.000612 x_2 - 1.6 \times 10^{-6} x_2^2 + 1.23 \times 10^{-7}\, x_1 x_2 \quad (4.4)$$

where x_1 is the defect size and x_2 is the shaft rotational speed.

Considering this equation, the predicted vibration level could be calculated. Fig. 4.13 can be integrated with the predicted vibration (peak-peak) level. Fig. 4.14 shows the predicted vibration levels graph for each defect size at different shaft rotational speeds as well as the actual vibration levels graph.

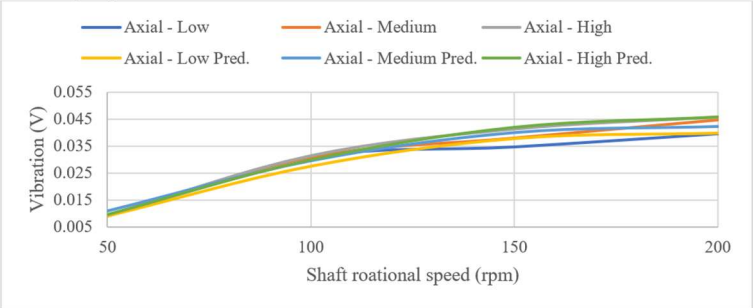

Fig. 4.14. Peak-peak vibration (actual and predicted)

Fig. 4.14 presents an insightful visualization of a comparative analysis between predicted and actual vibration levels across varying defect sizes and shaft rotational speeds. The predicted vibration levels graphs intricately overlay the predicted outcomes based on the regression analysis, while the actual vibration levels graph reflects empirical data obtained from tested observations. The collocation of these two datasets shows a clear degree of alignment between theoretical predictions and practical manifestations. Figs. 4.15 and 4.16 show the defect size line fit plot and the rotational speed line fit plot, respectively.

Figs. 4.15 and 4.16 collectively show a multi-layered investigation into the relationship between defect size estimated at varying rotational speeds and vibration levels as an investigation of anticipated and real vibration information. They express a relationship in a scatter plot of actual and predicted data points. Fig. 4.15 shows how diverse defect sizes impact vibration levels, whereas Fig. 4.16 shows how changes in the rotational speed of the wind turbine shaft correspond to changes in the vibration level of the turbine.

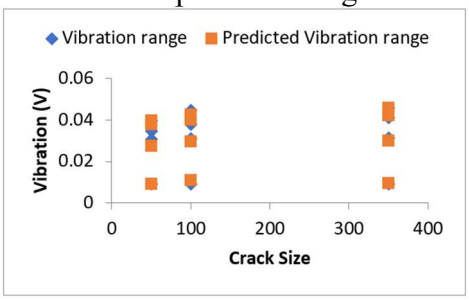

Fig. 4.15. Defect size line fit plot

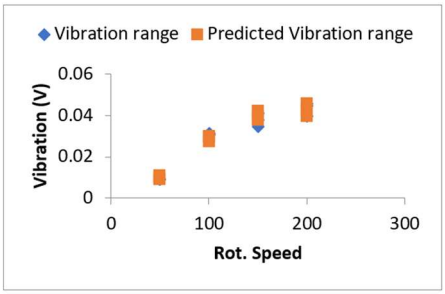

Fig. 4.16. Rotational speed line fit plot

4.5. Taguchi analysis

In this Taguchi analysis, the focus is on understanding the relationship between vibration range and crack size concerning rotational speed. Table 4.7 shows the response table for Signal to Noise Ratios (considering smaller vibration is better). This Table 4.7 shows the Signal to Noise Ratios (SNR) for two factors: crack size and rotational speed. The smaller the ratio, the better the quality. It indicates less variation or noise in the output. The factors are tested at different levels, denoted as 1, 2, 3, and 4. Delta represents the difference between the best and worst SNR for each factor. Rank indicates the ranking of each factor based on Signal to Noise ratios. Fig. 4.17 shows the main effects plot for SNR.

The other consideration of Taguchi analysis is the Response Table for Means, shown in Table 4.8. This Table 4.8 shows the means for crack size and rotational speed. The means indicate the average values of the factors at different levels. Delta represents the difference between the best and worst means for each factor. Rank indicates the ranking of each factor based on the mean values. Fig. 4.18 shows the Main effects plot for means.

Table 4.7. Response Table for Signal to Noise Ratios

Level	Crack Size	Rot. Speed
1	32.07	40.77
2	31.59	30.17
3	31.33	28.43
4		27.28
Delta	0.74	13.49
Rank	2	1

Table 4.8. Response Table for Means

Level	Crack Size	Rot. Speed
1	0.028550	0.009150
2	0.030685	0.031002
3	0.031844	0.037963
4		0.043325
Delta	0.003294	0.034175
Rank	2	1

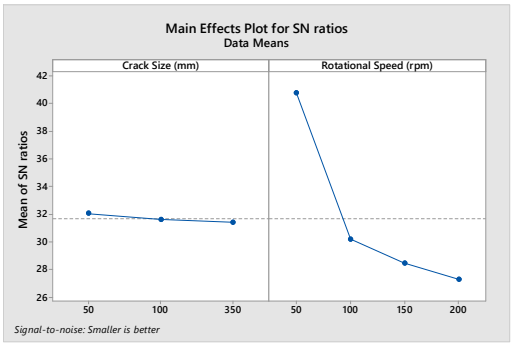

Fig. 4.17. Main effects plot for SN ratios

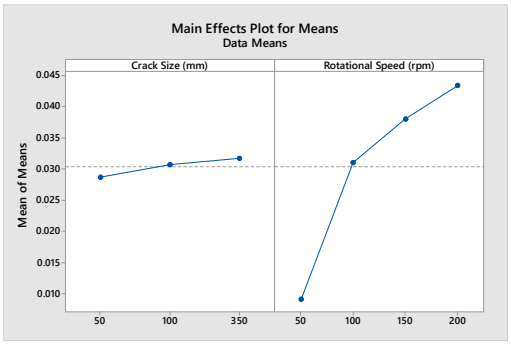

Fig. 4.18. Main effects plot for means

Taguchi analysis results can be interpreted as follows:

4.5.1. Crack Size:

In terms of Signal to Noise Ratio (SNR), the best performance is achieved at level 2, where the SNR is 31.59, indicating less variation in the output. In terms of means, the best performance is also at level 2, with a mean value of 0.030685. Therefore, for crack size, level 2 performs the best in both SNR and mean values.

4.5.2. Rotational Speed:

In terms of SNR, the best performance is at level 3, with an SNR of 28.43. In terms of means, the best performance is at level 1, with a mean value of 0.009150. Therefore, for rotational speed, there is a discrepancy between the optimal level based on SNR and mean values. Level 3 is optimal based on SNR, while level 1 is optimal based on mean values.

4.5. Prediction, Optimization and Sensitivity Analysis

The regression analysis determines the relationship between vibration responses and independent factors (crack size and rotational speed) by using defined regression algorithms and relationship estimates [19]. From the regression analysis shown in Table 4.6, the P-value for the shaft rotational speed is 0.000185 (<0.05) which is fine, but the P-value for the crack size is 0.412133 (>0.05). For optimization, the P-value of the crack size is high and should be excluded in regression analysis. The longer bar represents the input that contributes more to the model.

Considering the prediction and optimization of the multiple regression model, the following terms are in the fitted equation that models the relationship between vibration range and the rotation speed variables (x2: Rotational Speed and x2^2). The model fits the data well. Consequently, this equation can be used to predict the vibration range for specific values of the x variables and find the settings for the x variables that correspond to a desired value or range of values for the vibration range. The final model equation is:

$$Vibration\ range\ =\ -0.01762 + 0.000631x_2 + 0.000002x_2^2 \quad (4.5)$$

The model-building sequences in Fig. 4.19 display the order in which terms were added or removed in the regression model.

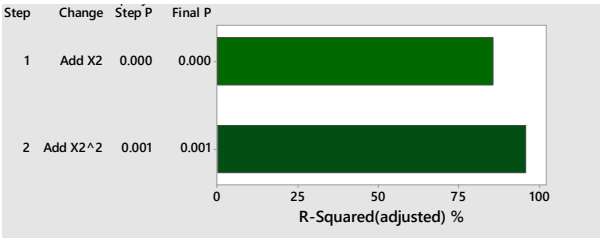

Fig. 4.19. Model building sequences

The final regression model equation shows that the relationship between the variables in the model is statistically significant ($p<0.1$) with 96.65% of the variation in vibration range can be explained by the regression model

5. CONCLUSION

The results of this study provide an important understanding of how vibration patterns are affected by axially defective wind turbine blades, with significant implications for improving maintenance and operating reliability. Through time-domain analysis, the study revealed a noticeable increase in vibration amplitude corresponding to the increased rotational speeds and defect severity levels. This trend underscores the essential role of rotational speed as a primary determinant of vibration level, with defects exacerbating the vibrational response. Utilizing analytical techniques such as regression analysis, a robust correlation between defect size, rotational speed, and vibration levels was established, with the regression model demonstrating a commendable explanatory power (R Square = 0.981841). Additionally, Taguchi analysis discerned optimal parameter settings for mitigating vibration-induced risks, guiding how to reduce operational disturbances and improve wind turbine performance. Furthermore, predictive and optimization models derived from regression analysis present actionable insights for targeted involvement strategies aimed at the limitation of vibration-related hazards. This research underscores the potential for proactive management of wind turbine integrity by integrating advanced analytical methodologies, thereby fostering sustained operational efficiency and reliability within renewable energy systems. The research findings contribute to advancing the understanding of wind turbine dynamics and asses performance and longevity while ensuring safety and sustainability in wind energy production, thereby supporting the continued growth of renewable energy technologies.

ACKNOWLEDGEMENT

The authors are thankful to the Faculty of Engineering at Sohar University for their guidance and cooperation.

COMPETING INTERESTS

The authors declare that they have no competing interests relevant to this research paper.

AVAILABILITY OF DATA AND MATERIALS

Materials used in this study are available upon reasonable request from the corresponding author.

REFERENCES

[1] Ogaili, A. A. F., Jaber, A. A., & Hamzah, M. N. (2023). Wind turbine blades fault diagnosis based on vibration dataset analysis, *Data in Brief*, **49**, 109414, doi: 10.1016/j.dib.2023.109414
[2] Zhou, F., Yang, J., Pang, J., & Wang, B. (2023). Research on control methods and technology for reduction of large-scale wind turbine blade vibration, *Energy Reports*, **9**, 912–923, doi: 10.1016/j.egyr.2022.12.042
[3] Pacheco, J., Pimenta, F., Guimarães, S., Castro, G., Cunha, Á., et al. (2024). Experimental evaluation of fatigue in wind turbine blades with wake effects, *Engineering Structures*, **300**, 117140, doi: 10.1016/j.engstruct.2023.117140
[4] Teng, W.; Ding, X.; Tang, S.; Xu, J.; Shi, B., et al. (2021). Vibration Analysis for Fault Detection of Wind Turbine Drivetrains – A Comprehensive Investigation, *Sensors 2021*, **21**, 1686, doi: 10.3390/s21051686
[5] Liu, X., Lü, C., Shi, L., Godbole, A. R., & Chen, Y. (2015). Influence of the vibration of large-scale wind turbine blade on the aerodynamic load, *Energy Procedia*, **75**, 873–879. doi: 10.1016/j.egypro.2015.07.196
[6] Xiao, F., Tian, C., Wait, I. W., Yang, Z., Still, B., et al. (2020). Condition monitoring and vibration analysis of wind turbine, *Advances in Mechanical Engineering*, **12**(3), 168781402091378, doi: 10.1177/1687814020913782
[7] Kaushik, N. V., & Shankar, N. N. (2022). Statistical Analysis using Taguchi Method for Designing a Robust Wind Turbine, *Journal of Advanced Research in Fluid Mechanics and Thermal Sciences*, **100**(3), 92–105, doi: 10.37934/arfmts.100.3.92105
[8] Pane, M., & Saragih, R. (2024). Optimal design of Gorlov turbine using computational fluid dynamics and Taguchi method, *VANOS Journal of Mechanical Engineering Education*, **9**(1), 25, doi: 10.30870/vanos.v9i1.24496
[9] Boukenoui, R., Bradai, R., & Kheldoun, A. (2024). A Taguchi method-based optimization algorithm for the analysis of the wind driven-self-excited induction generator, *International Journal of Power Electronics and Drive Systems/International Journal of Electrical and Computer Engineering*, **15**(2), 769, doi: 10.11591/ijpeds.v15.i2.pp769-783
[10] Koulocheris, D., Gyparakis, G., Stathis, A., & Costopoulos, T. N. (2013). Vibration signals and condition monitoring for wind turbines, *Engineering*, **5**(12), 948–955, doi: 10.4236/eng.2013.512116
[11] Song, D., Li, Z., Wang, L., Jin, F., Huang, C., et al. (2022). Energy capture efficiency enhancement of wind turbines via stochastic model predictive yaw control based on intelligent scenarios generation, *Applied Energy*, **312**, 118773, doi: 10.1016/j.apenergy.2022.118773
[12] Hayat, K., De Lecea, A. G. M., Moriones, C. D., & Ha, S. K. (2016). Flutter performance of bend–twist coupled large-scale wind turbine blades, *Journal of Sound and Vibration*, **370**, 149–162, doi: 10.1016/j.jsv.2016.01.032
[13] Chen, B., Zhang, Z., Hua, X., Nielsen, S. R., & Basu, B. (2018). Enhancement of flutter stability in wind turbines with a new type of passive damper of torsional rotation of blades, *Journal of Wind Engineering and Industrial Aerodynamics*, **173**, 171–179, doi: 10.1016/j.jweia.2017.12.011
[14] Liu, T. (2015). Classical flutter and active control of wind turbine blade based on piezoelectric actuation, *Shock and Vibration*, **2015**, 1–13, doi: 10.1155/2015/292368
[15] Imran, R. M., Hussain, D. M. A., Soltani, M., & Rafaq, R. M. (2016). Optimal tuning of multivariable disturbance-observer-based control for flicker mitigation using individual pitch control of wind turbine, *IET Renewable Power Generation*, **11**(8), 1121–1128, doi: 10.1049/iet-rpg.2016.0448
[16] Han, B., Zhou, L., Yang, F., & Xiang, Z. (2016). Individual pitch controller based on fuzzy logic control for wind turbine load mitigation, *IET Renewable Power Generation*, **10**(5), 687–693, doi: 10.1049/iet-rpg.2015.0320

[17] Zhang, Y., Cheng, M., & Chen, Z. (2015). Load mitigation of unbalanced wind turbines using PI-R individual pitch control, *IET Renewable Power Generation*, **9**(3), 262–271, doi: 10.1049/iet-rpg.2014.0242
[18] Dai, Y., Xie, F., Li, B., Wang, C., & Shi, K. (2023). Effect of blade tips ice on vibration performance of wind turbines, *Energy Reports*, **9**, 622–629, doi: 10.1016/j.egyr.2022.12.092
[19] Popović, B. (2019). The optimal solution to the problems by regression analysis, *Journal of Engineering Management and Competitiveness*, **9**(1), 25–37, doi: 10.5937/jemc1901025p

